RSC Advances

PAPER

View Article Online
View Journal | View Issue

Cite this: *RSC Adv.*, 2025, **15**, 35883

Tuning polyaniline doped with poly (4-styrenesulfonic acid) (PANI : PSS) as a nano-drug carrier for insulin delivery

Rawita Morarad,[a] Phimchanok Sakunpongpitiporn, *[ab] Kornkanok Rotjanasuworapong,[a] Nophawan Paradee,[ac] Walaiporn Prissanaroon-Ouajai[ad] and Anuvat Sirivat *[a]

Received 11th July 2025
Accepted 14th September 2025

DOI: 10.1039/d5ra04956c

rsc.li/rsc-advances

Polyaniline (PANI) is one of the most well-known conductive polymers, but it is not soluble in water. PSS, a polyelectrolyte and dopant, has demonstrated the ability to enhance both electrical conductivity and solubility in water. PANI : PSS were synthesized under the effect of polymerization times, oxidant (APS) ratios, and dopant (PSS) ratios. The suitable synthesized PANI : PSS was the ANI : APS mole ratio of 1 : 1 and ANI : PSS wt ratio of 1 : 5 for 24 h providing the highest electrical conductivity ($6.84 \times 10^{-2} \pm 4.30 \times 10^{-4}$ S cm^{-1}) and still remained as nanoparticles (42.11 ± 7.41 nm). Insulin, a model drug, was ion-exchanged with PANI : PSS, replacing PSS. The amount of insulin loaded into PANI : PSS (insulin-PANI : PSS) was varied with weight ratios of 0.5 : 1, 1 : 1, and 3 : 1, with the 1 : 1 wt ratio exhibiting 96.4% loading efficiency. The synthesized PANI : PSS is demonstrated as a potential insulin carrier for transdermal drug delivery.

1 Introduction

Conductive polymers (CPs) have been explored for more than two decades because their distinct electrical and optical properties make them valuable in various applications.[1,2] CPs possess not only the properties of traditional polymers, but also the ability to conduct electricity within their characteristically conjugated structures.[3] The most widely known CPs are polyacetylene, polyaniline, polypyrrole, and polythiophene.[4] CPs have been used in several applications, namely, fuel cells, supercapacitors, coatings, biomedical applications such as biosensors, and drug delivery.[5–13] Presently, there are many materials that possess electrical conductivity used in various applications. In 2023, Liu *et al.* investigated multilayered $Ti_3C_2T_x$ MXene/nano-hydroxyapatite to deliver doxorubicin hydrochloride (DOX).[14] In 2025, Mokhtari *et al.* developed $Ti_3C_2T_x$ MXene/AgNP modified poly(vinylidene fluoride-*co*-trifluoroethylene) P(VDF-TrFE) for use in a piezoelectric sensor.[15] In this work, a conductive polymer, which possessed high solubility in water, high biocompatibility, and no toxicity to human skin, was used as a drug carrier.

Polyaniline (PANI) can be easily synthesized to provide high electrical conductivity.[16] In addition to conventional redox doping, PANI can be doped with proton acids, which is known as proton doping.[17] However, conventional PANI does not dissolve in common solvents, resulting in processing limitations. The solubility of PANI can be improved by doping PANI with suitable counterions or by modifying PANI's chemical structure.[18] The counterions used to improve PANI solubility were dodecylbenzenesulfonic acid (DBSA),[19,20] camphorsulfonic acid (CSA),[19] and poly(4-styrenesulfonic acid) (PSS).[21] These counterions are large molecules that can provide steric hindrance and electrostatic stabilization for PANI molecules to avoid interparticle interaction and subsequent aggregation. There have been several reports on improving the solubility of PANI. Cadosa *et al.* synthesized PANI : CSA and PANI : DBSA to improve the solubility in toluene and THF. PANI : DBSA exhibited improved electrical properties compared with PANI : CSA.[19] Tang *et al.* synthesized water-soluble PANI : PSS and investigated its antibacterial performance.[21] To improve PANI water solubility, PSS is one candidate of various counterions as it is a water-soluble polymer. PSS acts as a polyelectrolyte due to its ionic nature. It can undergo interactions with oppositely charged species, leading to complexation or the formation of stable compounds. The mechanism of PANI synthesis is shown in Scheme 1.

Insulin is a hormone synthesized by the pancreas to manage blood sugar levels.[22] Insulin consists of 51 amino acids: the A

[a]*Conductive and Electroactive Polymers Research Unit, The Petroleum and Petrochemical College, Chulalongkorn University, Bangkok 10330, Thailand. E-mail: anuvat.s@chula.ac.th*

[b]*Center of Excellence in Sustainable Engineering, Mahanakorn University of Technology, Bangkok 10530, Thailand. E-mail: phimchanok@mut.ac.th*

[c]*Sustainable Polymer & Innovative Composite Materials Research Group, Department of Chemistry, Faculty of Science, King Mongkut's University of Technology Thonburi, Bangkok 10140, Thailand*

[d]*Department of Industrial Chemistry, Faculty of Applied Science, King Mongkut's University of Technology North Bangkok, Bangkok 10800, Thailand*

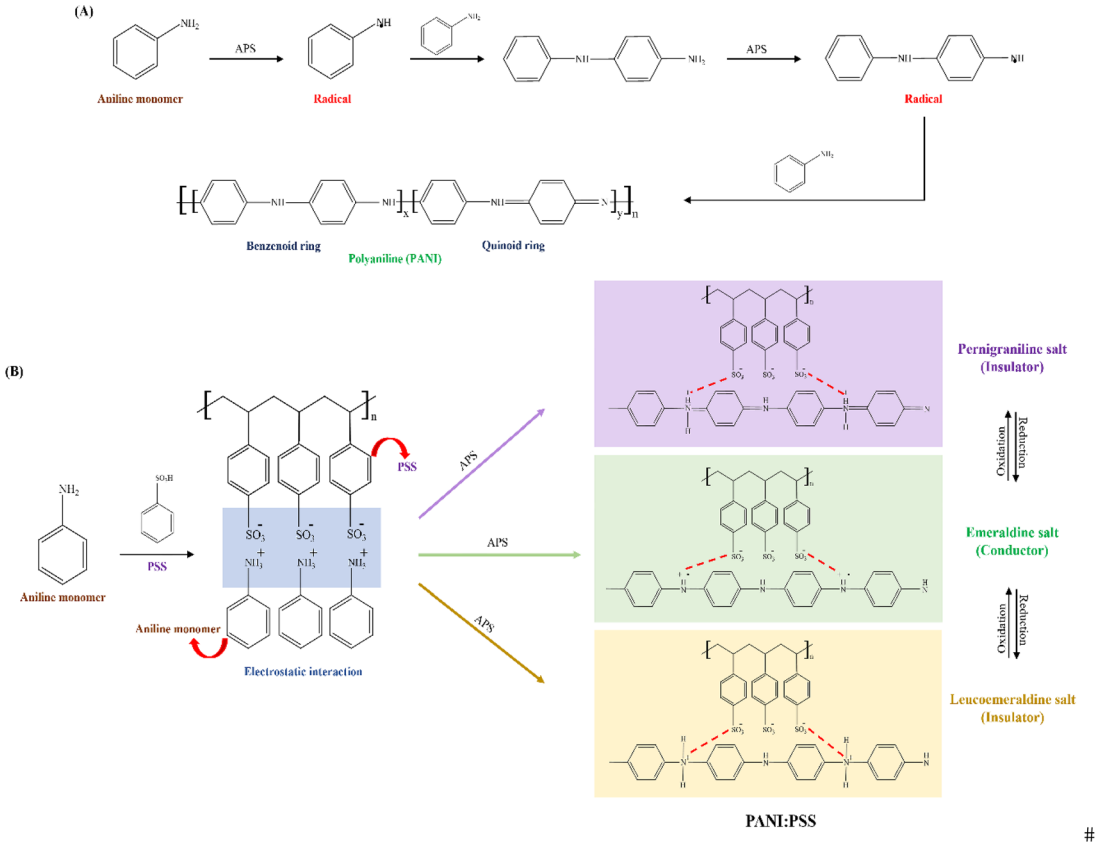

Scheme 1 Proposed mechanisms of (A) PANI polymerization and (B) PANI : PSS polymerization.

chain has 21 amino acids and the B chain has 30 amino acids.[22] Normally, insulin needs to be injected in the subcutaneous tissue to treat patients with diabetes. An alternative administration to treat diabetes patients is by the transdermal insulin delivery. Islam *et al.* investigated transdermal insulin delivery by developing a microemulsion system to enhance insulin permeation. The developed microemulsion was also a potential nanocarrier for protein and peptide delivery.[23] Demir *et al.* investigated insulin delivery with a microneedle hydrogel patch constructed from gelatin methacrylate and molybdenum disulfide (MoS_2) nanosheets. This system provided a satisfactory way to deliver insulin.[24]

Herein, PANI : PSS was synthesized as a water-soluble conductive polymer and as an insulin carrier to enhance transdermal insulin delivery. In this work, the tasks were to synthesize PANI : PSS *via* chemical oxidative polymerization with different polymerization times, monomer to oxidant ratios (ANI : APS ratio), and monomer to dopant ratios (ANI : PSS ratio) to obtain the highest electrical conductivity, and to optimize the maximum amount of insulin loaded into PANI : PSS. The originality of the work lies in the synthesis of a water-soluble conductive polymer (PANI : PSS). As a drug carrier, it will be demonstrated that PANI : PSS interacts with insulin by electrostatic interaction, in which the amount of insulin loaded will be shown here to be adequate as a single dose for diabetes patient treatment.

2 Materials and methods

2.1 Materials

Aniline monomer (ANI; 99.5%) was obtained from Loba Chemie. Poly(4-styrenesulfonic acid) (PSS; 18 wt% in H_2O, M_w: 75 000 g mol^{-1}) and insulin (recombinant, expressed in yeast, M_w: 5800 g mol^{-1}) were purchased from Sigma Aldrich. Ammonium peroxodisulfate (APS; $(NH_4)_2S_2O_8$) was purchased from EMSURE. Sodium hydrogen carbonate ($NaHCO_3$) was obtained from ACS. All chemicals were of analytical reagent (AR) grades. Ethanol and distilled water (DI water) were used for washing the synthesized conductive polymer.

2.2 Synthesis of PANI and PANI : PSS nanoparticles

PANI : PSS was synthesized *via* chemical oxidative polymerization from the ANI monomer, with APS as an oxidant and PSS as a dopant.[17] First, PSS was mixed with DI water (90 mL) and stirred for 30 min at room temperature. ANI monomer (1 mL) was added to the PSS solution and stirred for 10 min at room temperature. The ANI : PSS wt ratios were 1 : 0, 1 : 1, 1 : 3, 1 : 5, 1 : 7, 1 : 9, and 1 : 11. APS, as an oxidant, was dissolved in DI water (10 mL) and stirred for 10 min. The ANI : APS mole ratios were 1 : 0.50, 1 : 0.75, 1 : 1.00, 1 : 1.25, 1 : 1.50, 1 : 2.00, 1 : 2.50, and 1 : 3.00. The APS solution was added to the ANI : PSS solution to initiate the polymerization. The reaction times were 12, 24, 36, 48, and 72 h. The compositions of all effects are shown in

Table 1 Electrical conductivity (σ) values, particle sizes and shapes of PANI : PSS at various conditions

Conditions	σ (S cm^{-1})	Particle sizes (nm)	Particle shapes	Polymer color
Effect of polymerization times (ANI : PSS 1 : 1 wt ratio, ANI : APS 1 : 1 mole ratio)				
PANI : PSS_12 h	$3.03 \times 10^{-3} \pm 2.22 \times 10^{-5}$	67.58 ± 10.14	Spherical	Dark green
PANI : PSS_24 h	$4.00 \times 10^{-3} \pm 1.15 \times 10^{-5}$	74.41 ± 10.38	Spherical	Dark green
PANI : PSS_36 h	$1.63 \times 10^{-3} \pm 5.31 \times 10^{-6}$	60.28 ± 11.08	Spherical	Dark green
PANI : PSS_48 h	$1.37 \times 10^{-3} \pm 6.22 \times 10^{-4}$	61.33 ± 8.53	Spherical	Dark green
PANI : PSS_72 h	$1.50 \times 10^{-3} \pm 4.06 \times 10^{-5}$	58.88 ± 8.47	Spherical	Dark green
Effect of ANI : APS mole ratios (ANI : PSS 1 : 1 wt ratio for 24 h)				
PANI : PSS_ANI : APS 1 : 0.50	—	51.35 ± 5.85	Spherical	Yellow
PANI : PSS_ANI : APS 1 : 0.75	$6.01 \times 10^{-5} \pm 2.91 \times 10^{-5}$	73.78 ± 11.14	Spherical	Light green
PANI : PSS_ANI : APS 1 : 1.00	$4.00 \times 10^{-3} \pm 1.15 \times 10^{-5}$	74.41 ± 10.38	Spherical	Dark green
PANI : PSS_ANI : APS 1 : 1.25	$3.10 \times 10^{-3} \pm 4.10 \times 10^{-5}$	59.73 ± 8.66	Spherical	Dark green
PANI : PSS_ANI : APS 1 : 1.50	$2.00 \times 10^{-3} \pm 1.31 \times 10^{-5}$	64.59 ± 10.16	Spherical	Dark green
PANI : PSS_ANI : APS 1 : 2.00	—	61.89 ± 11.01	Spherical	Blue
PANI : PSS_ANI : APS 1 : 2.50	—	58.65 ± 7.87	Spherical	Purple
PANI : PSS_ANI : APS 1 : 3.00	—	58.65 ± 9.18	Spherical	Purple
Effect of ANI : PSS wt ratios (ANI : APS 1 : 1 mole ratio for 24 h)				
PANI_ANI : PSS 1 : 0	$5.40 \times 10^{-4} \pm 1.40 \times 10^{-5}$	98.33 ± 26.23	Fibrous	Dark green
PANI : PSS_ANI : PSS 1 : 1	$4.00 \times 10^{-3} \pm 1.15 \times 10^{-5}$	74.41 ± 10.38	Spherical	Dark green
PANI : PSS_ANI : PSS 1 : 3	$5.20 \times 10^{-2} \pm 1.80 \times 10^{-4}$	44.74 ± 9.79	Spherical	Dark green
PANI : PSS_ANI : PSS 1 : 5	$6.84 \times 10^{-2} \pm 4.30 \times 10^{-4}$	42.11 ± 7.41	Spherical	Dark green
PANI : PSS_ANI : PSS 1 : 7	$5.58 \times 10^{-2} \pm 1.02 \times 10^{-3}$	35.79 ± 5.99	Spherical	Dark green
PANI : PSS_ANI : PSS 1 : 9	$5.70 \times 10^{-2} \pm 7.07 \times 10^{-3}$	35.53 ± 6.02	Spherical	Dark green
PANI : PSS_ANI : PSS 1 : 11	$3.88 \times 10^{-2} \pm 5.95 \times 10^{-3}$	—	Spherical fusion	Dark green

Table 1. After the polymerization, the PANI : PSS solutions were centrifuged at 8000 rpm for 15 min. Dark green powders were obtained in the emeraldine salt form. They were washed with ethanol and DI water, then dried at 70 °C overnight.

2.3 Characterization of PANI and PANI : PSS nanoparticles

Fourier-Transform Infrared Spectroscopy (FT-IR; Nicolet, iS5) was used to determine the functional groups between 700 and 3500 cm^{-1} in the transmission mode with 64 scans. Simultaneous Thermal Analysis (STA; NETZSCH, STA 409) was used to investigate the thermal stability between 35–800 °C with a heating rate of 10 °C min^{-1} in a nitrogen atmosphere. An X-ray Diffractometer (XRD; Rigaku, SmartLab) was used to determine the crystallinity of the conductive polymers in the 2θ range between 10–50° with a scan rate 2° min^{-1} and a scan step of 0.1°. A Field Emission Scanning Electron Microscope (FE-SEM; Hitachi, S-4800) was used to observe the surface morphology. The samples were first coated with platinum for 200 s to improve electrical conductivity. SEM images were recorded at a magnification of 700 00× and at 5.0 kV. An energy-dispersive X-ray spectrometer (EDX) combined with a field-emission scanning electron microscope (FE-SEM; Hitachi, S-4800) was used to determine the elemental composition and distribution. X-ray Photoelectron Spectroscopy (XPS; Kratos Analytical, Axis Ultra DLD) was used to determine the elemental compositions and doping levels of the conductive polymers. UV-vis spectrophotometry (Tecan, The Infinite 200 PRO NanoQuant) was used to investigate the UV-vis absorbance values of the 3 different chemical structures of PANI : PSS. A 4-point probe (Lucas-Signatone Pro4) was used to measure the electrical conductivity.

2.4 Optimum amount of insulin loading into PANI : PSS nanoparticles (insulin-PANI : PSS)

PANI : PSS with the ANI : APS 1 : 1 mole ratio and ANI : PSS 1 : 5 wt ratio for 24 h (1.10 mg) was mixed with DI water (50 μL) at 50 °C until a homogeneous solution was obtained. Insulin (0.55, 1.10, and 3.30 mg) was dissolved in 125 mM $NaHCO_3$ (50 μL) at room temperature. Then, various insulin solutions were mixed with the PANI : PSS solution and stirred for 24 h at room temperature. The insulin-PANI : PSS was characterized by FT-IR analysis to determine the functional groups and to identify interactions between the insulin and the PANI : PSS, and by STA to investigate the thermal stability of the insulin and the insulin-PANI : PSS. The loading efficiency of insulin in the PANI : PSS was calculated using eqn (1):[25]

$$\text{Loading efficiency (\%)} = \frac{\text{loaded insulin}}{\text{initial insulin added}} \times 100 \quad (1)$$

The loaded insulin amount in the PANI : PSS carrier was determined by UV-vis at 274 nm and calculated from the calibration curve between insulin concentration (x-axis) and absorbance (y-axis).[26]

3 Results and discussion

3.1 FT-IR spectra of PANI and PANI : PSS nanoparticles

The FTIR spectrum of PANI is shown in Fig. 1A(a). The PANI bands are at 3300–3100, 1561 and 1495, 1306, and 1122 cm^{-1}, corresponding to the N–H stretching vibration of the secondary aromatic amine, C=C stretching vibrations of the quinoid (N=

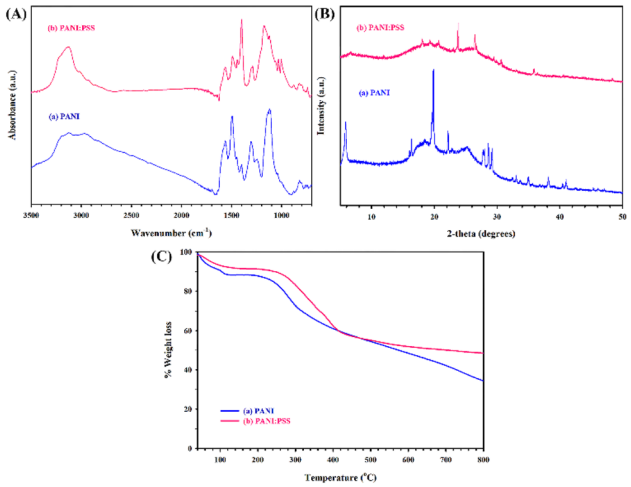

Fig. 1 Characterization of PANI and PANI : PSS synthesized with an ANI : APS 1 : 1 mole ratio and ANI : PSS 1 : 5 wt ratio for 24 h: (A) FTIR spectra, (B) XRD patterns, and (C) TGA thermograms.

Q═N) and benzenoid (N═B═N) units from the oxidized PANI, aromatic C–N stretching vibration of the benzenoid unit, and in-plane vibration of C–H in the benzene ring of the quinoid unit, respectively.[27–30] The FTIR spectrum of PANI : PSS, as shown in Fig. 1A(b), reveals new bands at 1174/1124 cm^{-1} and 1032/1005 cm^{-1}, corresponding to the symmetric- and antisymmetric-stretching bands of the SO_3^{2-} group from the PSS.[29] The results suggest that PSS was incorporated into PANI to form PANI : PSS.

Considering the effect of polymerization times, none of the PANI : PSS spectra were significantly different. For the effect of ANI : APS mole ratios as shown in Fig. S1A, at higher ANI : APS ratios (Fig. S1A(f)–(h)), the FTIR spectra with the peaks at around 3300 to 3000 cm^{-1} exhibit strong intensities due to the –N–H stretching from the over oxidation by the excessive APS. Moreover, the peaks at 1581 and 1502 cm^{-1} and at 1124 and 1038 cm^{-1} exhibit weak intensities as the excess of APS could obscure the interaction between PANI and PSS.

For the effect of ANI : PSS wt ratios, as shown in Fig. S1B, at higher PSS amounts, the characteristic bands of PANI at 1555 and 1473 cm^{-1} show weak intensities because the excess PSS obscures the PANI bands. The characteristic bands of PSS at 1032 and 1005 cm^{-1} show moderately strong intensities as higher amounts of PSS were added.

3.2 XRD diffractograms of PANI and PANI : PSS nanoparticles

The diffractograms of PANI and PANI : PSS under various conditions are shown in Fig. 1B. The PANI diffractogram in Fig. 1B(a) exhibits a broad peak, suggesting the semi-crystalline nature of PANI.[31] A sharp peak centered around $2\theta \approx 20°$ suggests the periodic alignment parallel to the polymer chains, indicating the semi-crystalline structure.[32] The PANI diffractogram exhibits a sharp peak at $2\theta \approx 6°$, corresponding to the more ordered structures between parallel planes of the stacked PANI backbones.[33,34] For the PANI : PSS diffractogram in Fig. 1B(b), the sharp peak at $2\theta \approx 20°$ disappears. This indicates that the disorder of the PANI chain increased due to the interaction between PANI and PSS.[35] The sharp peak at $2\theta \approx 6°$ disappeared, suggesting that PSS was incorporated into the PANI, resulting in highly disordered PANI backbones.

Considering the effect of polymerization times, none of the PANI : PSS diffractograms were significantly different. For the effect of ANI : APS mole ratios as shown in Fig. S1C, revealed that the peak at $2\theta \approx 20°$ became sharper with higher amounts of APS, and new peaks at $2\theta \approx 16°$ and 33° appeared, possibly resulting from the characteristic peaks of the excess APS.[36]

Considering the effect of ANI : PSS wt ratios, as shown in Fig. S1D, the intensity of the peak at $2\theta \approx 20°$ decreases with higher amounts of PSS because PANI : PSS adopted more amorphous structures as the interaction between PANI and PSS disrupted the regular packing of the polyaniline chains, and the hydrophilic nature of PSS introduced more water or other solvents into the system, disrupting the crystallinity. The diffractograms of PANI : PSS with ANI : PSS ratios of 1 : 3 to 1 : 11 wt, as shown in Fig. S1D(c)–(g), show new peaks at $2\theta \approx 24°$ and 26°, corresponding to the π–π stacking interactions of the conjugated PANI chains.[30]

3.3 Thermal stability

The thermal stability profiles of PANI and PANI : PSS are shown in Fig. 1C. PANI exhibits a one-step degradation temperature at 281.6 °C due to the PANI backbone degradation.[35] PANI : PSS exhibits a two-step degradation at temperatures of 336.2 °C and 391.5 °C due to the degradation of the PSS side chain and the PANI backbone, respectively.[35,37] It can be seen that the PANI degradation temperature shifted from 281.6 °C to 391.5 °C (PANI : PSS), as the electrostatic interaction between PANI and PSS produced a more compact structure.[38]

3.4 UV-vis

The UV-vis spectra of PANI : PSS with 3 different chemical structures, namely, leucoemeraldine, emeraldine, and pernigraniline, are shown in Fig. 2A. The leucoemeraldine structure exhibits only one peak at 400–450 nm, corresponding to the π–π* transitions in the benzenoid rings.[39] This structure has a minimal visible absorption, resulting in a pale or yellow color of PANI : PSS. The emeraldine structure exhibits 2 peaks at 400–450 nm and 800–900 nm, corresponding to the π–π* transitions of the benzenoid rings and π–polaron transition (free carrier tail), respectively.[40–43] This structure absorbs light in the red region, resulting in the characteristic green color of the PANI : PSS. The pernigraniline structure exhibits 2 peaks at 400–450 nm and 600–700 nm, corresponding to the π–π* transitions in the quinoid rings and the Peierls gap transition, respectively.[40,44] The Peierls effect in conductive polymers is a phenomenon in which a conducting stage undergoes a transition to an insulating stage due to lattice distortion, leading to an increase in the Fermi level.[45] This structure absorbs light in the yellow-green region, giving the PANI : PSS a blue to violet color.[46]

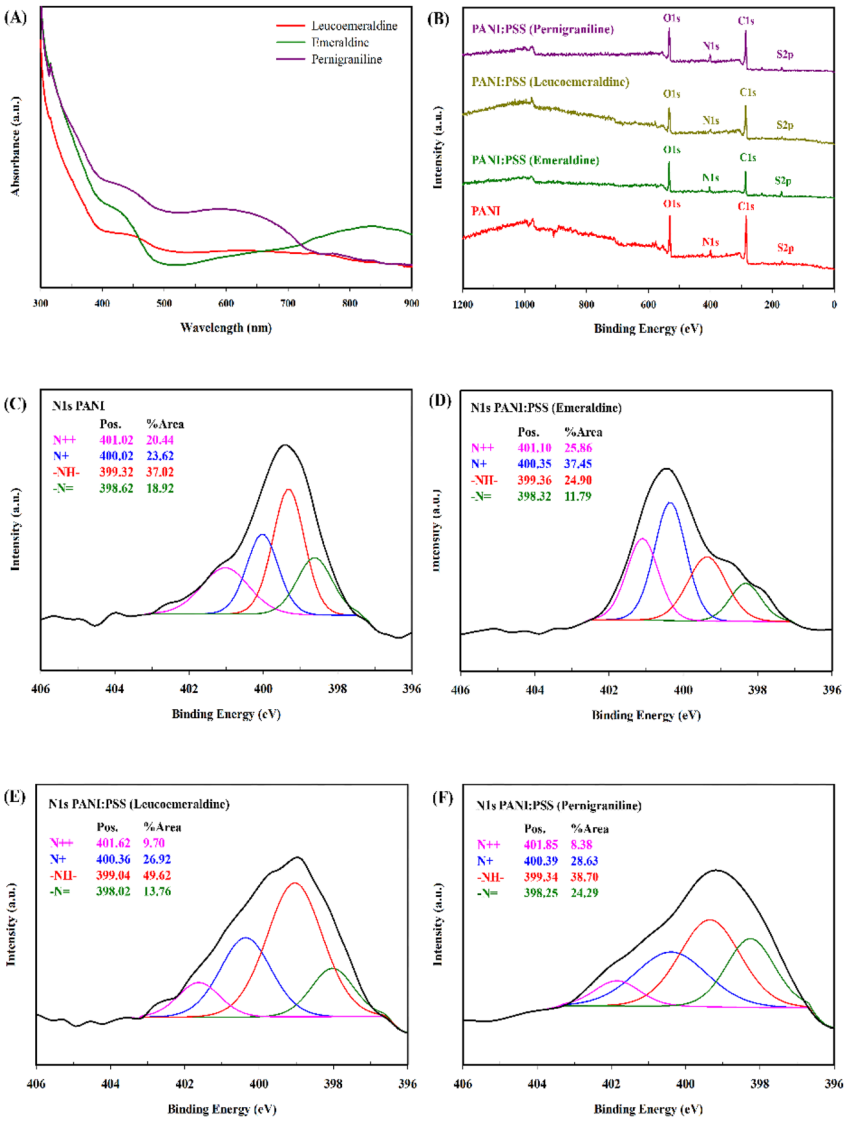

Fig. 2 (A) UV-VIS spectra of PANI : PSS with various structures; (B) XPS survey scans of PANI and PANI : PSS with various structures; and high-resolution XPS N 1s spectra of (C) PANI, (D) PANI : PSS (emeraldine), (E) PANI : PSS (leucoemeraldine), and (F) PANI : PSS (pernigraniline).

3.5 XPS analysis

The elemental compositions of PANI and PANI : PSS with different structure forms were investigated by XPS. The survey scan spectra and percentage elemental compositions are shown in Fig. 2B and Table S1, respectively. The S element increased from 1.50% (PANI) to 5.09% (PANI : PSS, emeraldine) because of the incorporation of PSS as the dopant. This result confirms the successful synthesis of PANI : PSS. The N 1s spectra of PANI and PANI : PSS are shown in Fig. 2C–F. These spectra were deconvoluted into four Gaussian component peaks due to different nitrogen bonding environments. They can be attributed to the protonated imine (=NH^+; N1), protonated amine (–NH_2^+; N2), neutral amine (–NH^-; N3), and neutral imine (–N=; N4) centered at 401, 400, 399, and 398 eV, respectively.[47–49] The oxidation states were determined by the intensity ratios of the neutral imine to neutral amine (N4/N3); a ratio of 0.50 indicates the emeraldine form.[46] In Fig. 2C and D, the ratios of 0.51 and 0.47 correspond to the emeraldine form, indicating the half-oxidation state. In Fig. 2E, the ratio of 0.28 corresponds to the leucoemeraldine form, indicating the low oxidation state. In Fig. 2F, the ratio of 0.68 corresponds to the pernigraniline form, indicating the high oxidation state.[48,50] The doping levels were calculated from the intensity ratios of N^+/N (all N^+ species to the total nitrogen).[47,50] They are 44.06%, 63.31%, 36.62%, and 37.01% for PANI, PANI : PSS (emeraldine), PANI : PSS (leucoemeraldine), and PANI : PSS (pernigraniline), respectively. These results are to be correlated with the electrical conductivity.

3.6 SEM images of PANI and PANI : PSS nanoparticles

The particle sizes and shapes of PANI and PANI : PSS nanoparticles are tabulated in Table 1. The surface morphologies of PANI in Fig. 3a and PANI : PSS in Fig. 3b–(e) show fibrous and spherical shapes, respectively. By using PSS, spherical micelles were formed, leading to the spherical shape of PANI : PSS.[51]

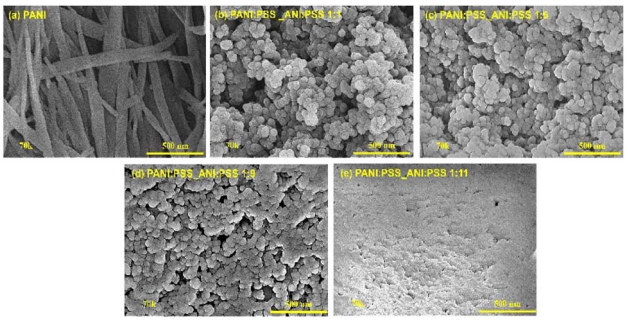

Fig. 3 SEM images: (a) PANI and PANI : PSS with ANI : PSS wt ratios of (b) 1 : 1, (c) 1 : 5, (d) 1 : 9, and (e) 1 : 11.

Considering the effect of polymerization times, the particle size decreased with increasing polymerization times, because PSS interacted more with PANI over a longer time.[52] Studying the effect of ANI : APS mole ratios, the size of the PANI : PSS nanoparticles slightly decreased with increasing APS amount, because a higher APS amount reacted more with the PANI.[53]

Considering the effect of ANI : PSS wt ratios, the particle size of PANI : PSS decreased with increasing PSS amount as more PSS interacted with the PANI.[54,55] At an ANI : PSS ratio of 1 : 11, the PANI : PSS particles tended to stick together, forming a spherical fusion. The largest PANI : PSS nanoparticle found was 74.41 ± 10.38 nm. Larger PANI : PSS nanoparticles would be expected to induce higher electrical conductivity from a more favorable PANI : PSS formation.[56,57]

3.7 Electrical conductivity (σ) of PANI and PANI : PSS nanoparticles

The σ values of PANI : PSS synthesized under various conditions are shown in Table 1 and Fig. 4A. Considering the effect of polymerization times, the electrical conductivity values for PANI : PSS at 12 h and 24 h are $3.03 \times 10^{-3} \pm 2.22 \times 10^{-5}$ and $4.00 \times 10^{-3} \pm 1.15 \times 10^{-5}$ S cm^{-1}, because the longer polymerization time enhances the aniline monomer conversion, leading to improved PANI formation when compared to a shorter time of 12 h.[57]

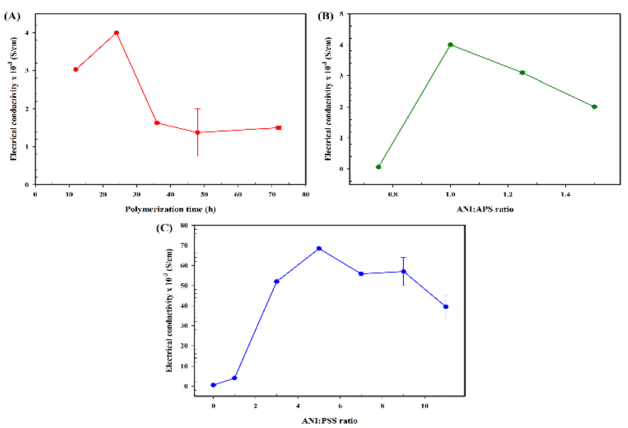

Fig. 4 Electrical conductivity (σ) values of PANI : PSS under the effects of: (A) times; (B) ANI : APS ratios; and (C) ANI : PSS ratios.

There was a report that the σ value increased as the crystallinity and molecular weight of PANI increased.[52] From the SEM images, the PANI : PSS particle size also increased at 24 h. As the polymerization time was extended from 24 to 72 h, there was a tendency for σ to decrease as both PANI and PSS reached their equilibrium reactions within 24 h, and the excess PANI formation could lead to polymer aggregation.[57] Therefore, a suitable polymerization time for PANI : PSS was 24 h.

Considering the effect of ANI : APS mole ratios, the σ of PANI : PSS increased with increasing ANI : APS ratio and decreased after reaching the optimum ANI : APS ratio of 1 : 1, as shown in Table 2 and Fig. 4B.[54] In Fig. 4B, there are 2 regimes of PANI : PSS electrical conductivity. The first regime is for ANI : APS mole ratios of 1 : 0.50, 1 : 0.75, and 1 : 1.00. The electrical conductivity was not measurable at the lowest ANI : APS ratio of 1 : 0.50 due to the fully reduced form of PANI, known as the leucoemeraldine salt.[15] Increasing the ANI : APS ratio to 1 : 0.75, and 1 : 1.00, the σ values were $6.01 \times 10^{-5} \pm 2.91 \times 10^{-5}$ and $4.00 \times 10^{-3} \pm 1.15 \times 10^{-5}$ S cm^{-1}, respectively, as PANI was in the half-oxidized form, known as the emeraldine salt.[17,59] The second regime is for ANI : APS mole ratios from 1 : 1.0 to 1 : 1.50, for which the σ value decreased from $4.00 \times 10^{-3} \pm 1.15 \times 10^{-5}$ to $2.00 \times 10^{-3} \pm 1.31 \times 10^{-5}$ S cm^{-1}, respectively; the electrical conductivity was not measurable at ANI : APS ratios above 1 : 1.50. This was due to a shorter conjugation length produced at high oxidant concentrations, leading to the deterioration in electrical conductivity as the PANI chains entered the over-oxidation state (fully oxidized PANI), known as the pernigraniline salt.[17,60] The proposed mechanisms of PANI and PANI : PSS are shown in Scheme 1. Therefore, the suitable ANI : APS mole ratio for PANI : PSS synthesis was 1 : 1.

Considering the effect of the ANI : PSS wt ratio (Table 1 and Fig. 4C), the σ values of PANI_ANI : PSS 1 : 0 and PANI_ANI : PSS 1 : 1 are $5.40 \times 10^{-4} \pm 1.40 \times 10^{-5}$ S cm^{-1} and $4.00 \times 10^{-3} \pm 1.15 \times 10^{-5}$ S cm^{-1}, respectively.[58] PSS acted as a dopant to increase the number of charge carriers (holes) and hence reduced the band gap between the conduction and valence bands.[61] At higher PSS concentrations, the σ value increased due to increasing number of holes until it reached the optimum PANI : PSS with an ANI : PSS ratio of 1 : 5. For PANI : PSS materials with ANI : PSS ratios above 1 : 5, the σ value decreased as the polymer chain structure was disrupted at very high dopant concentrations.[62,63] The highest σ value for PANI : PSS was $6.84 \times 10^{-2} \pm 4.30 \times 10^{-4}$ S cm^{-1}. Therefore, the suitable ANI : PSS wt ratio for PANI : PSS synthesis was 1 : 5.

3.8 Insulin-PANI : PSS

To confirm the presence of insulin and the interaction between insulin and PANI : PSS synthesized with an ANI : APS 1 : 1 mole ratio and an ANI : PSS 1 : 5 wt ratio for 24 h, FTIR and STA thermal analyses were utilized; the results are shown in Fig. 5A and B. The FTIR bands of pure insulin are observed at 3285, 1640, and 1512 cm^{-1} due to the –N–H stretching and the C=O stretching vibration of amide I and amide II, which are

Table 2 The UV-vis data of insulin amount

Samples	Initial insulin added (mg)	Insulin amount loaded into PANI : PSS (mg)	Loading efficiency (%)
PANI : PSS (control)	0	0	—
Insulin-PANI : PSS (0.5 : 1.0)	0.55	0.51	92.7%
Insulin-PANI : PSS (1.0 : 1.0)	1.10	1.06	96.4%

characteristic of proteins, respectively.[64,65] The FTIR spectrum of insulin-PANI : PSS shows peaks at 1303, 1176, 1127, 1036, and 1008 cm^{-1} from PANI : PSS. The peaks at 1653 and 1507 cm^{-1} can be seen as occurring from insulin. The peaks at 3285 cm^{-1} from insulin and at 3128 cm^{-1} from PANI : PSS are overlapped to 3233 cm^{-1}, and the band of pure insulin is slightly shifted from 1640 cm^{-1} to 1653 cm^{-1}, suggesting an electrostatic interaction occurring between the negatively charged ions of insulin and the positively charged ions of PANI. In contrast, the insulin-PANI : PSS sample prepared *via* powder mixing shows the characteristic bands of individual insulin and PANI : PSS.

The insulin-PANI : PSS samples prepared *via* electrostatic interaction exhibited a 3-step degradation with increasing temperatures, as shown in Fig. 5B and Table S2; the steps correlate to moisture evaporation below 100 °C, degradation of PSS and insulin around 250–350 °C, and degradation of the PANI chain around 400–500 °C. With increasing amounts of insulin from 0.5 to 1.0, the degradation temperature for the PANI chain shifted to higher values as the insulin interacted with PANI and improved the thermal stability of the PANI. However, there was no shift in the PANI main chain degradation temperature when the amount of insulin was increased to 3.0, as the insulin and PANI : PSS interaction reached the optimum amount. In contrast, the insulin-PANI : PSS sample prepared by powder mixing also exhibited a 3-step degradation at temperatures similar to those of the insulin-PANI : PSS samples prepared *via* the electrostatic interaction between the negatively charged ions of insulin and the positively charged ions of PANI, the PANI chain degradation temperature did not shift to higher or lower values, meaning that there were no interactions between the insulin and PANI : PSS in the sample generated *via* powder mixing.

The XPS survey scan and narrow N 1s spectra of insulin-PANI : PSS are shown in Fig. 5C and D. The survey scan shows Na 1s, O 1s, N 1s, C 1s, and S 2p peaks at 1073, 532, 400, 285, and 169 eV, respectively. The Na 1s came from the solvent, namely, the $NaHCO_3$ solution used to dissolve insulin. The percentage of S element decreased from 5.09% to 1.63% after insulin was incorporated by ion exchange, which confirms the successful loading of insulin into the PANI : PSS.

The distribution of N element in PANI and insulin-PANI : PSS was confirmed *via* EDX mapping, as shown in Fig. 6. The

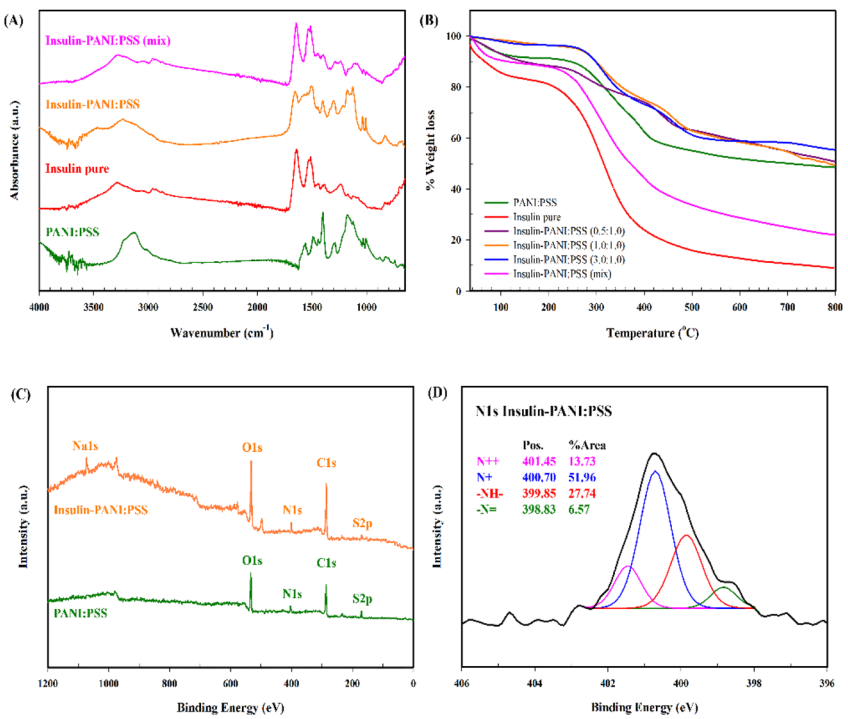

Fig. 5 Characterization of insulin-PANI : PSS: (A) FTIR spectra, (B) thermograms, (C) XPS survey scans, and (D) N 1s spectrum of insulin-PANI : PSS.

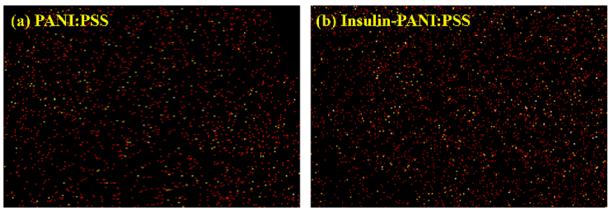

Fig. 6 EDX mapping of the N element: (a) PANI : PSS and (b) insulin-PANI : PSS.

insulin-PANI : PSS mapping (Fig. 6b) demonstrates the increase and homogeneous distribution of N element. This indicates that insulin was successfully loaded onto PANI : PSS.

4 Conclusions

In summary, PANI : PSS, a water-soluble conductive polymer, was successfully synthesized *via* chemical oxidative polymerization with the highest electrical conductivity of $6.84 \times 10^{-2} \pm 4.30 \times 10^{-4}$ S cm^{-1} at an ANI : APS 1 : 1 mole ratio and an ANI : PSS 1 : 5 wt ratio for 24 h. Insulin, a model drug, was successfully loaded into PANI : PSS at 96.4% loading efficiency using an initial insulin to PANI : PSS wt ratio of 1 : 1. Insulin and PANI : PSS interacted *via* electrostatic interactions through ion exchange between insulin and PSS ions. The amount of insulin loaded into PANI : PSS has been shown here to be sufficient for a single dose for patients with diabetes.

Author contributions

Rawita Morarad: methodology, investigation, writing-original draft. Phimchanok Sakunpongpitiporn: writing-review & editing. Kornkanok Rotjanasuworapong: writing-review & editing. Nophawan Paradee: writing-review & editing. Walaiporn Prissanaroon-Ouajai: writing-review & editing. Anuvat Sirivat: writing-review & editing, supervision.

Conflicts of interest

There are no conflicts to declare.

Data availability

Data will be made available on request.

Supplementary information: FTIR spectra and XRD diffractograms of PANI:PSS under the effects of: (A) and (C) ANI : APS mole ratios; and (B) and (D) ANI : PSS wt ratios. SEM images of PANI : PSS synthesized at various polymerization times and ANI : APS mole ratios. Elemental compositions from XPS survey scan spectra of PANI and PANI : PSS with different structure forms. Thermal analysis data of the insulin-PANI : PSS. See DOI: **https://doi.org/10.1039/d5ra04956c**.

Acknowledgements

This work was funded by the Petroleum and Petrochemical College, the 100th Anniversary Chulalongkorn University Fund for Doctoral Scholarship, the 90th Anniversary of Chulalongkorn University Scholarship, the Conductive and Electroactive Polymers Research Unit (CEAP), and the Thailand Science Research and Innovation Fund, Chulalongkorn University (TSRI-CU), and the National Research Council of Thailand (NRCT).

References

1 R. A. Green and J. A. Goding, in *11 – Biosynthetic Conductive Polymer Composites for Tissue-Engineering Biomedical Devices*, ed. L. Poole-Warren, P. Martens and R. Green, Woodhead Publishing Series in Biomaterials, Number 107, Cambridge, 2016, pp. 277–298.
2 T. Nezakati, A. Seifalian, A. Tan and A. M. Seifalian, *Chem. Rev.*, 2018, **118**(14), 6766–6843.
3 V. Nassiet, B. Hassoune-Rhabbour, O. Tramis and J.-A. Petit, 22 – Electrical and electronics, in *Adhesive Bonding: Science, Technology and Applications*, R. D. Adams, Woodhead Publishing Series in Welding and Other Joining Technologies, Cambridge, 2nd edn, 2021, 719–761.
4 L. S. Kuznetsova, V. A. Arlyapov, Y. V. Plekhanova, S. E. Tarasov, A. S. Kharkova, E. A. Saverina and A. N. Reshetilov, *Polymers*, 2023, **15**(18), 3783.
5 S. Ghosh, S. Das and M. E. G. Mosquera, *Polymers*, 2020, **12**(12), 2993.
6 N. Mahato, H. Jang, A. Dhyani and S. Cho, *Polymers*, 2020, **12**(11), 2480.
7 G. A. Snook, P. Kao and A. S. Best, *J. Power Sources*, 2011, **196**(1), 1–12.
8 M. G. Tadesse, A. S. Ahmmed and J. F. Lübben, *J. Compos. Sci.*, 2024, **8**(2), 53.
9 M. Goyal, K. Singh and N. Bhatnagar, *Prog. Org. Coat.*, 2024, **187**, 108083.
10 B. Lakard, *Appl. Sci.*, 2020, **10**(18), 6614.
11 T. Acar, K. N. Çimen, E. Özalp, Ö. Ilıca and E. A. Özerol, *ChemistrySelect*, 2023, **8**(30), e202300819.
12 A. Puiggalí-Jou, L. J. del Valle and C. Alemán, *J. Controlled Release*, 2019, **309**, 244–264.
13 M. E. Alkahtani, M. Elbadawi, C. A. R. Chapman, R. A. Green, S. Gaisford, M. Orlu and A. W. Basit, *Adv. Healthcare Mater.*, 2024, **13**(3), e2301759.
14 X. Liu, R. Sun, Z. Zhou and Y. Tang, *J. Mater. Sci. Technol.*, 2023, **180**, 91–101.
15 F. Mokhatari, R. W. Symes, Z. Simon, B. Dharmasiri, L. C. Henderson, M. M. Joosten and R. J. Varley, *J. Mater. Chem. A*, 2025, **13**, 6482–6492.
16 L. S. B. Upadhyay, S. Rana and N. Kumar, in *Chapter 20 – Nanomaterials in Tissue Engineering: Applications and Challenges*, ed. A. D. Talukdar, S. D. Sarker and J. K. Patra, Elsevier Inc., Amsterdam, 2022, pp. 533–554.
17 M. Beygisangchin, S. Abdul Rashid, S. Shafie, A. R. Sadrolhosseini and H. N. Lim, *Polymers*, 2021, **13**(12), 2003.

18 J. Liu, X. Hu, X. Wang, J. Yao, D. Sun, Z. Fan and M. Guo, *Polym. Int.*, 2013, **63**(4), 722–726.
19 M. J. R. Cadosa, M. F. Santos Lima and D. M. Lenz, *Mater. Res.*, 2007, **10**(4), 425–429.
20 V. Kumar, T. Yokozeki, T. Goto and T. Takahashi, *Polymer*, 2016, **86**, 129–137.
21 H. Tang, Y. Liu, B. Li, B. Shang, J. Yang, C. Zhang, L. Yang, K. Chen, W. Wang and J. Liu, *Bioact. Mater.*, 2021, **6**(12), 4758–4771.
22 G. Wilcox, Insulin and insulin resistance, *Clin. Biochem. Rev.*, 2005, **26**(2), 19–39.
23 M. R. Islam, S. Uddin, M. R. Chowdhury, R. Wakabayashi, M. Moniruzzaman and M. Goto, *ACS Appl. Mater. Interfaces*, 2021, **13**(36), 42461–42472.
24 B. Demir, L. Rosselle, A. Voronova, Q. Pagneux, A. Quenon, V. Gmyr, D. Jary, N. Hennuyer, B. Staels, T. Hubert, A. Abderrahmani, V. Plaisance, V. Pawlowski, R. Boukherroub, S. Vignoud and S. Szunerits, *Nanoscale Horiz.*, 2022, **7**(2), 174–184.
25 A. H. Khalbas, T. M. Albayati, N. S. Ali and I. K. Salih, *S. Afr. J. Chem. Eng.*, 2024, **50**, 261–280.
26 K. Tari, S. Khamoushian, T. Madrakian, A. Afkhami, M. J. Łos, A. Ghoorchian, M. R. Samarghandi and S. Ghavami, *Int. J. Mol. Sci.*, 2021, **22**, 12479.
27 S. Xiong, Y. Wang, Y. Lu, H. Li, J. Liu, S. Li, Z. Qiu, M. Gong, B. Wu, J. Chu, X. Wang and R. Zhang, *Polym. Bull.*, 2018, **75**, 3427–3443.
28 P. Jayamurugan, R. Mariappan, S. Deivanayaki, V. Ponnuswamy, P. Maadeswaran, M. Chavali and Y. V. Subba Rao, *Polym. Compos.*, 2020, **28**(8–9), 645–653.
29 S. Uzunçar, L. Meng, A. P. F. Turner and W. C. Mak, *Biosens. Bioelectron.*, 2021, **171**, 112725.
30 Y. Wang, S. Wu, Q. Yin, B. Jiang and S. Mo, *Polym. Test.*, 2021, **94**, 107017.
31 K. C. Sajjan, M. Faisal, B. S. Khened and S. Khasim, *Int. J. Electr. Electron. Eng.*, 2013, **2**(2), 67–76.
32 R. Kandulna and R. B. Choudhary, *Optik*, 2017, **144**, 40–48.
33 P. Anilkumar and M. Jayakanan, *Langmuir*, 2006, **22**, 5952–5957.
34 M. R. Husin, A. Arsad, S. S. Suradi, O. Alothman, N. Ngadi and M. J. Kamaruddin, *Chem. Eng. Trans.*, 2017, **56**, 1012–1020.
35 F. P. Du, Q. Q. Li, P. Fu, Y. F. Zhang and Y. G. Wu, *J. Mater. Sci.: Mater. Electron.*, 2018, **29**, 8666–8672.
36 A. Idboufrade, B. Bouargane, B. Ennasraoui, B. Mohamed Ghali, A. Bachar, B. Bakiz, A. Ali and S. Billah, *Waste Biomass Valorization*, 2022, **13**, 1795–1806.
37 V. G. Kulkarni, L. D. Campbell and W. R. Mathew, *Synth. Met.*, 1989, **30**(3), 321–325.
38 L. M. Huang, C. H. Chen, T. C. Wen and A. Gopalan, *Electrochim. Acta*, 2006, **51**(13), 2756–2764.
39 K. Bienkowski, Polyaniline and its Derivatives Doped with Lewis Acids – Synthesis and Spectroscopic Properties, PhD thesis, Faculty of Chemistry, Université Joseph-Fourier – Grenoble I; Warsaw University of Technology, 2006.
40 S. B. Yoon, E. H. Yoon and K. B. Kim, *J. Power Sources*, 2011, **196**, 10791–10797.
41 C. W. Kuo, Z. Y. Kuo, J. J. Jow, T. Y. Wu, J. Y. Chen and X. X. Zhu, *Int. J. Electrochem. Sci.*, 2012, **7**, 4974–4987.
42 S. Gul, A. A. Shah and S. Bilal, *J. Phys.:Conf. Ser.*, 2013, **439**, 012002.
43 C. Dhivya, S. Anbu Anjugam Vandarkuzhali and N. Radha, *Arabian J. Chem.*, 2019, **12**(8), 3785–3798.
44 A. A. Nekrasov, V. F. Ivanov and A. V. Vannikov, *Electrochim. Acta*, 2001, **46**, 4051–4056.
45 S. A. Brazovskii, N. N. Kirova and S. I. Matveenko, *J. Exp. Theor. Phys.*, 1984, **86**, 743–757.
46 M. L. Mota, A. Carrillo, A. J. Verdugo, A. Olivas, J. M. Guerrero, E. C. De la Cruz and N. Noriega Ramírez, *Molecules*, 2019, **24**(8), 1621.
47 M. M. Mahat, D. Mawad, G. W. Nelson, S. Fearn, R. G. Palgrave, D. J. Payne and M. M. Stevens, *J. Mater. Chem. C*, 2015, **3**, 7180–7186.
48 Y. Y. Smolin, M. Soroush and K. K. S. Lau, *J. Nanotechnol.*, 2017, **8**, 1266–1276.
49 V. Lyutov, V. Kabanova, O. Gribkova, A. Nekrasov and V. Tsakova, *Polymers*, 2020, **12**, 1050.
50 S. Golczak, A. Kanciurzewska, M. Fahlman, K. Langer and J. J. Langer, *Solid State Ionics*, 2008, **179**, 2234–2239.
51 P. Sakunpongpitiporn, K. Phasuksom, N. Paradee and A. Sirivat, *RSC Adv.*, 2019, **9**, 6363–6378.
52 T. V. Freitas, E. A. Sousa, G. C. Fuzari Jr and E. P. S. Arlindo, *Mater. Lett.*, 2018, **224**, 42–45.
53 Z. Taghipour, H. Eisazadeh and M. Tanzifi, *Int. J. Eng., Trans. B*, 2014, **27**, 227–238.
54 A. Abdelmagid, A. El Tahan, M. Habib, M. Anas and M. Soliman, *Synth. Met.*, 2020, **259**, 116232.
55 A. Montes-Rojas, M. Ramírez-Orizaga, J. G. Ávila-Rodríguez and L. M. Torres-Rodríguez, *Membranes*, 2020, **10**, 387.
56 P. C. Maity and M. Khandelwal, *Am. J. Mater. Synth. Process.*, 2016, **1**(4), 37–42.
57 H. Abu Hassan Shaari, M. M. Ramli, M. M. A. B. Abdullah, M. N. Mohtar, N. Abdul Rahman, A. Ahmad, N. H. Osman and F. Rusydi, *Sustainability*, 2022, **14**(14), 8940.
58 R. Morarad, W. Naeowong and A. Sirivat, *Drug Delivery Transl. Res.*, 2024, **14**(4), 280–293.
59 B. Qiu, J. Wang, Z. Li, X. Wang and X. Li, *Polymers*, 2020, **12**(2), 310.
60 J. Deng, X. Wang, J. Guo and P. Liu, *Ind. Eng. Chem. Res.*, 2014, **53**, 13680–13689.
61 X. Guo, Y. Sun, X. Sun, J. Li, J. Wu, Y. Shi and L. Pan, *Macromol. Rapid Commun.*, 2024, **45**(1), 2300246.
62 I. Rahayu, D. R. Eddy, A. R. Novianty, Rukiah, A. Anggreni, H. Bahti and S. Hidayat, *IOP Conf. Ser.:Mater. Sci. Eng.*, 2019, **509**, 012051.
63 L. M. Yuningsih, D. Mulyadi and I. Aripandi, *Am. J. Mater. Sci.*, 2017, **7**(3), 59–63.
64 A. Prusty and S. K. Sahu, *ISRN Nanotechnol.*, 2013, 591751.
65 B. V. Farahani, H. Ghasemzadeh and S. Afraz, *J. Chin. Chem. Soc.*, 2016, **63**(5), 438–444.